Moroccan Journal of Chemistry
ISSN: 2351-812X
http://revues.imist.ma/?journal=morjchem&page=login
Orimolade al. / Mor. J. Chem. 6 N°4 (2018) 721-735

Silica-coated magnetite nanoparticles as a novel adsorbent for the removal of Iron(II) and Manganese(II) from surface water: Equilibrium, kinetics and thermodynamic studies.

Benjamin Olawale ORIMOLADE[1,2]* Folahan Amoo ADEKOLA[1] and Ganiyu Babatunde ADEBAYO[1]

[1]*Department of Industrial Chemistry, University of Ilorin, P.M.B 1515, Ilorin, Nigeria*
[2]*Department of Applied Chemistry, University of Johannesburg, Doorfontein, 2198, South Africa*
,

* *Corresponding author:*
orimoladeben@yahoo.com
Received 11 Sep 2017,
Revised 07 Dec 2018,
Accepted 20 Dec 2018

Abstract

Silica-coated magnetite nanoparticle was synthesized as model adsorbent for the removal of Fe(II) and Mn(II) which are major contaminants of surface water. Prepared adsorbent was fully characterized using Fourier Transform Infra-red spectroscopy, Scanning Electron Microscopy, X-Ray Diffraction and X-Ray Fluorescence. The optimum conditions of adsorption were determined by investigating the effect of initial metal ion concentration, contact time, adsorbent dose, pH of aqueous solution and temperature. Adsorption equilibrium time was found to be 60 min for both Fe(II) and Mn(II). The equilibrium adsorption experimental data for the two metals were found to fit the Langmuir adsorption isotherms best with a regression value of 0.989 and 0.979 for Fe(II) and Mn(II) respectively. The pseudo second order kinetic model was found to describe the adsorption kinetics for both metals more effectively. The adsorption processes involving both metals were endothermic. The adsorbent was finally applied to typical raw water with initial manganese and iron concentrations of 1.45 mg/l and 3.67 mg/l, respectively, and the removal efficiency was 90 % for Mn and 47 % for Fe.

Keywords: *Magnetite, adsorption, isotherm, kinetic, Manganese and Iron*

1.Introduction

Several pollutants are being introduced to water bodies through natural means and improper discharge of untreated industrial effluents. The pollutants include metal ions such as iron and manganese ions. Manganese and iron are considered as emerging contaminants because they pose threat to human health and the environment [1, 2]. Free manganese ions are released in the water by means of the photochemical and chemical reduction of manganese oxides coming from organic matter while iron is commonly found in its oxide form in water. The exposure to high levels of manganese and iron causes decrease in fitness of organisms as well as neurological damage in humans [3, 4]. In water supplies, iron(II) and manganese (II) salts are uns**Table** and are precipitated as insoluble hydroxide, which settles out as a rust-coloured silt and such water causes staining in laundry. When water containing high amount of iron and manganese are used for industrial purposes like textile and paper production, the quality of the paper and textile produced are greatly reduced [5]. Therefore, removal of manganese and iron from water is necessary. Many techniques have been developed for removing heavy metals from water and wastewater and these include polyphosphate treatment, ion-exchange treatment, precipitations, ultrafiltration, adsorption and chlorination. Among these, adsorption technique stands out and is widely used in wastewater treatment [6]. Different kinds of adsorbents such as activated carbon and various biomaterials have been used in the past for the removal metal irons from water. For example, Nazar et al. studied the adsorption of Fe(II) , Cr(III) and Co(II) ions from aqueous solution by using Activated carbon prepared from *Mesquite* tree [7]. The adsorption behavior of rice husk ash with respect to manganese and iron has previously been reported by Adekola et al and the removal efficiency was 100 % for Mn and 70 % for Fe when the adsorbent was used on raw water [8]. Similarly, Yan et al. studied the adsorption of Fe and Mn onto magnetic grapheme oxide and observed a monolayer heterogenous and spontaneous adsorption process [9]. Due to recent advancement in nanotechnology, nano metal oxides are now being used as adsorbents for the removal of contaminants from water due to their relatively large surface area. The adsorptive behavior of bio-adsorbent can further be improve by incorporating them with nano metal oxides. Therefore, this research work studied the adsorptive removal of Fe(II) and Mn(II) from aqueous solution using synthesized silica-nanomagnetite composite material. The physicochemical parameters such as pH, adsorbent dose, temperature, initial concentration of metal ions and contact time affecting adsorption process were optimized. The kinetics and thermodynamic studies of the adsorption process were also carried out.

1. Materials and Method

2.1 Collection and Preparation of Rice Husk waste material

Rice-husk which is an agro-waste was collected from a rice milling center at a local market in North-Cental Nigeria. The rice husk was milled and washed with distilled water to remove all impurities. The material was then oven dried at 105 ^{0}C for 5 h. It was thereafter sieved using 300um sieve mesh. The material was then ashed at 550 ^{0}C in the muffle furnace [8].

2.2 Synthesis of Nano-magnetite

The reverse co-precipitation method used for the synthesis of the magnetite nano-particles. The iron salts solution was prepared by dissolving 3.24 g (0.02 moles) of $FeCl_3.6H_2O$ and 1.99 g (0.01 moles) of $FeCl_2.4H_sO$ in 20 mL de-ionized water at 25°C for 20 minutes. 8 mol/L of alkaline solution was prepared by adding 4.58 g of NaOH to 14 mL of de-ionized water and stirred for 30 minutes at 25°C. Magnetite nano particles were then precipitated by adding the iron salts solution drop-wisely into the NaOH solution at 80^{0}C with continuous stirring. The co-precipitated samples were washed with deionised water and acetone to remove the [10]. The overall chemical reaction may be indicated as follows:

$Fe^{2+} + 2\ Fe^{3+} + 8OH^{-} \rightarrow Fe_3O_4 + 4H_2O$

2.3 Synthesis of silica coated Fe_3O_4 nanoparticles:

Rice husk ash and nanomagnetite in the ratio of 1:1 were dispersed in 0.5M HCl to form slurry. The slurry was stirred and evaporated to dryness in an oven. The composite material was washed with deionised water, filtered and further dried in an oven at 100 ^{o}C for 12 hours [11]. The material was denoted as S-nM and used as the adsorbent.

2.4 Sorption Experiment

Batch experiments were used for the adsorption studies. This was done by contacting 0.1 g of the adsorbent with the 25 mL of Fe(II) and Mn(II) solutions and then agitated for 2 h. The adsorbent was then filtered from the solution and the concentration of Fe(II) and Mn(II) left in the solution taken. The quantity adsorbed (q_e) and percentage adsorbed were calculated using the equations 1 and 2 respectively.

$$q_e = \frac{(C_o - C_e)V}{W} \qquad 1$$

$$\%A = \frac{C_o - C_e}{C_o} X100 \qquad 2$$

C_o and C_e are the initial and equilibrium concentration of the metal ions respectively. V is the volume of Fe(II) and Mn(II) solutions used while W is the mass of adsorbent taken.

2.5 Adsorption isotherms studies

The experimental data were fitted into Langmuir, Freundlich, Temkin and Dubinin-Radushkevich adsorption isotherms. Langmuir isotherm describes quantitatively the formation of a monolayer adsorbate on the outer surface of the adsorbent, and after that no further adsorption takes place. The linear form Langmuir isotherm is given in equat 3.

$$\frac{1}{q_e} = \frac{1}{Q_0} + \frac{1}{Q_0 K_L C_e} \qquad 3$$

Q_0 (mg/g) and K_L (l/mg) are Langmuir constants related to adsorption capacity and rate of adsorption, respectively. The values of Q_0 and K_L were calculated from the slope and intercept of the Langmuir plot of $1/q_e$ versus $1/C_e$.

Freundlich adsorption isotherm describes the adsorption characteristics for the heterogeneous surface [12]. These data often fit the empirical equation proposed by Freundlich. The linear form is shown in equation 4.

$$\log Q_e = \log K_f + \frac{1}{n} \log C_e \qquad 4$$

K_f is Freundlich isotherm constant (mg/g), n is adsorption intensity. The constant K_f is an approximate indicator of adsorption capacity, while 1/n is a function of the strength of adsorption in the adsorption process. The Temkin isotherm model assumes that the adsorption energy decreases linearly with the surface coverage due to adsorbent–adsorbate interactions. The linear form can be expressed by equation 5. Where RT/b = B (J/mol), which is the Temkin constant related to heat of sorption, whereas A_T (l/g) represents the equilibrium binding energy, R (8.314 J/mol/K) is the universal gas constant at T (K) which is the absolute solution temperature.

$$q_e = \frac{RT}{b_T} ln A_T + \left(\frac{RT}{b}\right) ln C_e \qquad 5$$

2.6 Adsorption kinetics studies

The kinetics of the adsorption process were studied by analyzing the experimental data using Pseudo first order, pseudo second order, Elovich and Intra-particle diffusion models. The pseudo-first order model is expressed in equation 6.

$$\log(q_e - q_t) = \log q_e - \frac{K_{ad}\, t}{2.303} \qquad 6$$

qt (mg/g) is the amount adsorbed at any time t and k_{ad} (min^{-1}) is the equilibrium rate constant of pseudo first order adsorption. The values of k_{ad} and q_e are determined from the slope and intercept of the plot of log (q_e -q_t) versus t, respectively. The pseudo-second order model is based on assumption that sorption follows a second order mechanism as given in equation 7.

$$\frac{t}{q_t} = \frac{1}{K_{ad}\, q_e^{\,2}} + \frac{t}{q_e} \qquad 7$$

k_{ad} is the pseudo-second order rate constant (g/mg/min). The value of q_e is determined from the slope of the plot of t/q_t versus t. One of the most useful models for describing such 'activated' chemisorption is the Elovich model. The Elovich equation is given in equation 8 [13]. α is the initial adsorption rate, β is the desorption constant during each experiment at time t.

$$q_t = \frac{1}{\propto} \ln(\propto B) + \frac{1}{\propto} lnt \qquad 8$$

2.7 Statistical validity of the Kinetic and isotherm models

Statistical tools such as regression coefficient (R^2), sum of square error (SSE) and Chi-square test ($\chi 2$) were used to confirm the suitability and best fit among the kinetic models. Sum of square error (SSE) is the mostly used by researchers with the mathematical expression is given in equation 9.

$$SSE = \sum_{i=1}^{n} \left(q_{e,cal} - q_{e,exp}\right)^2 \qquad 9$$

The non-linear chi-square test is a statistical tool necessary for the best fit of an adsorption kinetics system. Better agreement between the experimental quantity adsorbed and the calculated quantity adsorbed can be judged using this tool. The mathematical expression is given in equation 10.

$$X^2 = \sum_{i=1}^{n} \frac{\left(q_{e,exp} - q_{e,cal}\right)^2}{q_{e,cal}} \qquad 10$$

2.8 Thermodynamic study

The thermodynamic parameters were obtained by varying the temperature conditions between 30 and 70 °C while keeping other variables constant including metal concentration, pH, adsorbent dose, contact time. The values of the thermodynamic parameters such as ΔG, ΔH, and ΔS, were calculated using the equations 11 – 13 [14].

$$\Delta G = -RT\ln K_d \qquad 11$$

$$\ln Kd = \Delta S/R - \Delta H/RT \qquad 12$$

$$\Delta G = \Delta H - T\Delta S \qquad 13$$

ΔG^o is the standard Gibb's free energy change for the adsorption (J/mol), R is the universal gas constant (8.314 J/mol/K) while T is the temperature (K). K_d is the distribution coefficient of the adsorbate The plot of ln K_d versus 1/T gives a straight line with the slope and the intercept giving values of ΔH and ΔS.

2. Results and Discussion

XRF elemental analysis

The X-Ray fluorescence analysis data (using Kevex Fisons Analyst 771) show the concentrations of important elements present in the synthesized materials (**Table** 1). The rice husk contained 92% silica (SiO_2). Previous researchers have also reported high silica content of rice husk ash [8,15]. The synthesized magnetite has 95% iron oxide content which was expected for magnetite. The percentage of the iron oxide and silica present in the composite material are 38% and 56% respectively according to **Table** 1.

Table 1. X-Ray Fluorescence of Rice Husk Ash, magnetite and composite material

Compounds	Rice Husk Ash	nanomagnetite	Composite
SiO_2	**92.64**	2.8	**55.6**
TiO_2	0.031	-	-
Fe_2O_3	0.27	-	-
Al_2O_3	0.269	0.99	-
MnO	0.072	0.30	0.091
CaO	1.60	0.12	0.231
MgO	0.828	-	-
Na_2O	0.73	-	-
Ag_2O	2.06	-	1.63
K_2O	0.75	0.042	0.314
P_2O_5	0.19	0.20	3.07
Eu_2O_3	0.43	0.54	0.28
Re_2O_7	0.12	0.10	0.06
V_2O_5	-	0.036	0.019
Cr_2O_3	-	0.056	0.030
Fe_3O_4	-	**94.51**	**38.48**
CuO	-	0.050	0.032
ZnO	-	0.061	0.02
In_2O_3	-	0.13	-
La_2O_3	-	0.10	0.099

Scanning Electron Microscopy

The surface morphology of the samples observed using Carl Zeiss Ultra plus field emission electron microscop are shown in **Figure** ures 1a and 1b. The SEM image of the magnetite shows that the particles were in aggregated form rather than existing as separate nanoparticles which could have been caused by the large surface area and magnetic dipole-dipole interactions of the individual particles [16]. The SEM image of the composite material as shown in **Figure** ures 1b revealed that the iron particles were surrounded by the silica particles which indicated that the nano particles of the magnetite are well coated with the silica. The surface of the composite material appeared to be rough and coarse with cracks which indicated that it will be a good adsorbent.

a

Figure 1a: SEM images of magnetite

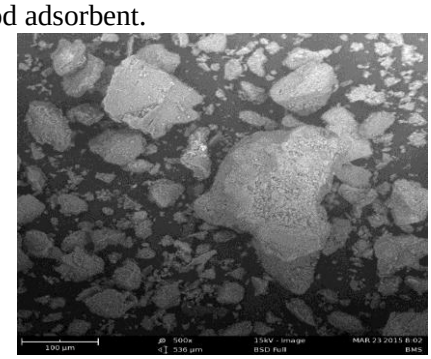

Figure ure 1b: SEM images SiO_2-nFe_3O_4 composite

X-Ray Diffraction

The samples were anlysed using X-Ray diffractometer (PW 3050/60 Goniometer). **Figure ure** 2a illustrates the XRD patterns of the synthesized nanomagnetite particles. The position and relative intensity of all diffraction peaks match well with those of the magnetite (JCPDS 19-629) and broad peaks indicates nano-crystalline nature of the particles. The XRD pattern of the rice husk silica has a peak between 20 – 30 degrees which confirms the amorphous nature of the silica (**Figure** 2b). **Figure ure** 2c shows XRD pattern of silica coated Fe_3O_4 nano-particles. Thus XRD pattern indicates the presence of amorphous silica coating on magnetite nanoparticles surface. The peak at 20-30 degree corresponds to SiO_2 and the rest of peaks are as those in XRD patterns of Fe_3O_4. It can be seen from **Figure ure** 2c that coating process of magnetite does not change the peak position corresponding to magnetite between 30 and 40 degree but rather the intensity of the peak.

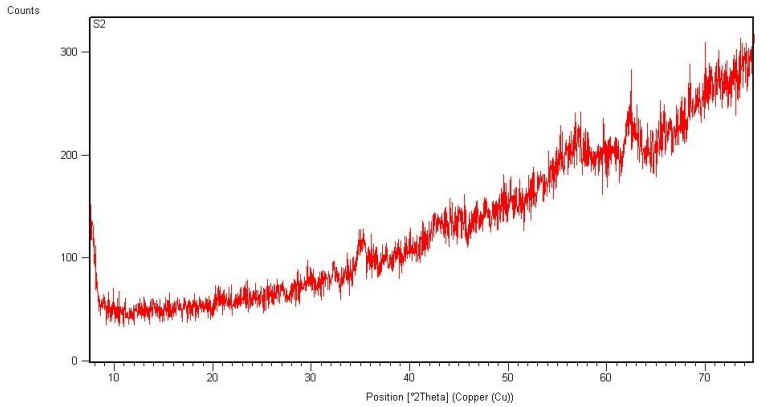

Figure ure 2a: XRD of synthesized nanomagnetite

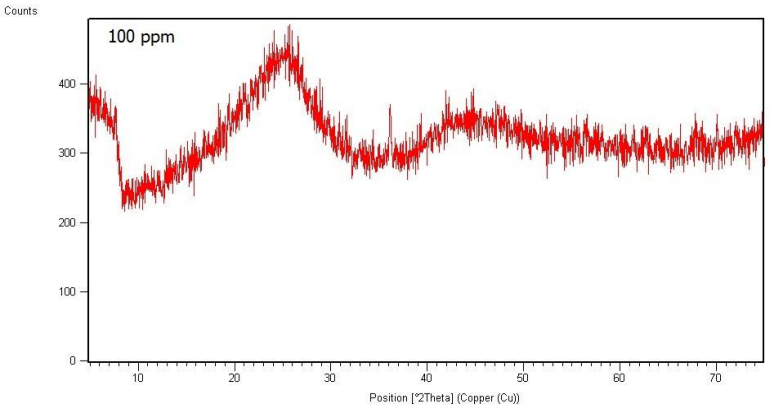

Figure ure 2b: XRD Pattern of Rice Husk Silica

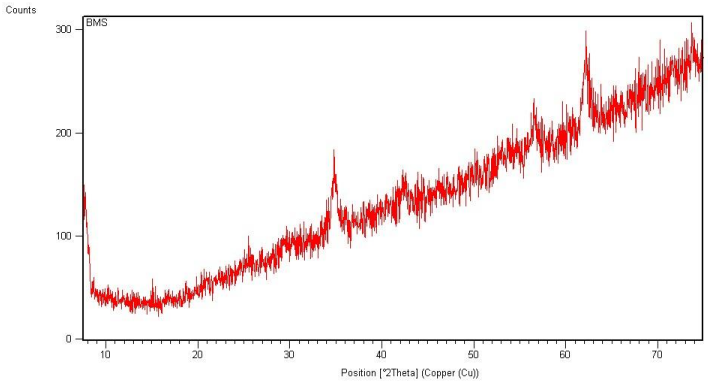

Figure ure 2c: XRD pattern of S-nM

Infra Red Spectroscopy

The IR spectra of the synthesized nanomagnetite and the silica-nanomagnetite are presented in **Figure** ures 3a and 3b respectively. The band at 565.14 cm^{-1} has been assigned to Fe-O bond and attributed to formation of ferrite phase (**Figure** .3a). Different from magnetite, FT-IR spectra of silica coated magnetite, (**Figure ure** 3b) shows pronounce changes, particularly at region of 1300–700cm^{-1}, indicating the presence of silica coating. The presence of silica coating on the nanomagnetite is shown with characteristic band at 464.84 cm^{-1} from bending vibration of Si-O-Si. FTIR band of 1099.43 cm^{-1} has been assigned to asymmetric bending vibration corresponding to Si-O-Si bond FTIR bands in coated magnetite FT-IR spectra around 1654.92cm^{-1} and 3427 cm^{-1} come from bending and stretching vibration, respectively, of –OH groups from both Fe-OH and Si-OH. Stretching vibration of Si-O-H bonding results in an absorbance band at 800.46 cm^{-1}. In FTIR spectra of magnetite coated only with silica, absence of Si-OH vibration band was due to overlap with broad band of stretching vibration from Si-O-Si.

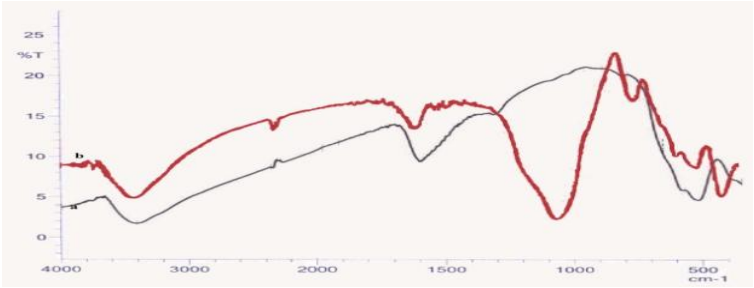

Figure ure 3: (a) FTIR spectra of nanomagnetite (b) FTIR spectra of SiO_2-nFe_3O_4

Results of Sorption Studies

Effect of Initial Concentration

The quantity of metals adsorbed by the adsorbent increased with initial concentration of the metal solution until equilibrium was reached. The highest amount of Fe(II) ion adsorbed was 1.79 mg/g at an initial concentration of 75ppm while the highest quantity of Mn(II) ion adsorbed was 9.08 mg/g at an initial concentration of 100 ppm (**Figure ure** 4). No further increase was observed beyond the equilibrium. This may be due to the lack of available active sites required for the high initial concentration of Fe(II) and Mn(II) [17,18]. The increase in adsorption capacity with an increase in initial Fe(II) and Mn(II) concentration is as a result of the increase in driving force due to the concentration gradient developed between the bulk solution and surface of the adsorbent [19]. At higher concentrations, the active sites of the adsorbents were surrounded by more Fe(II) and Mn(II) ions and the process of adsorption continues until equilibrium is reached.

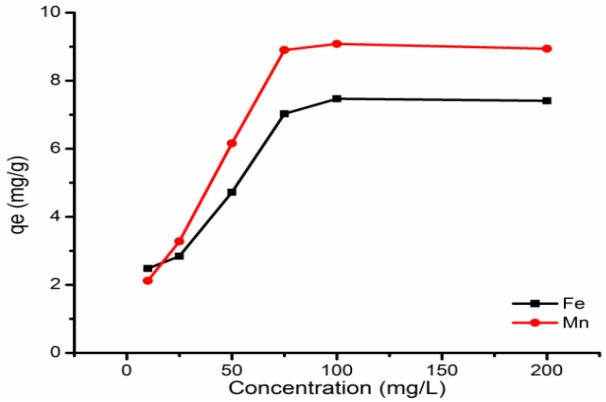

Figure . 4: Effect of concentration on the sorption capacity of Fe(II) and Mn(II) onto SnM (weight= 0.1g, pH 6, Temp= 30±2^{0}C for 240min)

Effect of pH

The effect of pH on the adsorption of Fe(II) and Mn(II) onto SnM was studied at pH 2–6 and pH 2-8 respectively and the results are presented in **Figure** 5. The pH range studied for the sorption of Fe(II) was limited to 6 because beyond this pH there was a precipitation of the metal hydroxide. It was observed that the percent removal was increased from 5 to 47% for Fe(II) ions and from 20 to 42% for Mn(II) ions, as pH was increased from 2 to 6. The maximum removal was found to be 47% for Fe(II) and 42% for Mn(II) ions at pH 6. This phenomenon could be partly attributed to the fact that when the pH values increased, adsorbent surfaces were more negatively charged and attracted metal ions with positive charges, thus causing the adsorption onto the adsorbent surface [20]. However adsorption efficiency decreased after attaining the maximum adsorption limit as a result of the formation of soluble hydroxylated complexes of the metal ions and their ionized nature. At higher pH levels, Fe(II) and Mn(II) would be converted into their hydroxide forms and get precipitated.

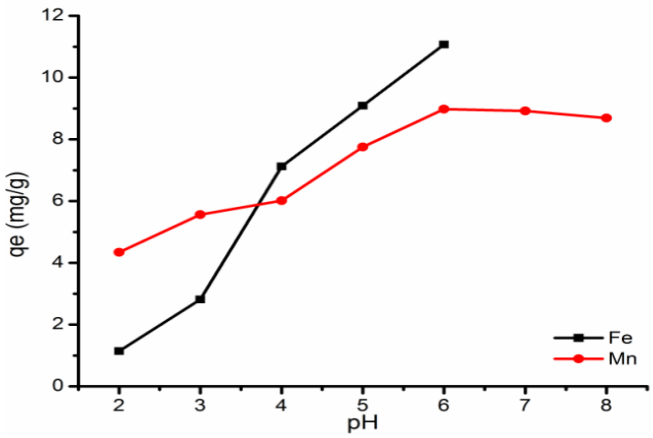

Figure . 5: Effect of pH on the sorption capacity of Fe(II) and Mn(II) onto S-nM (weight= 0.1g, Temp= 30±2^{0}C for 240min)

Effect of Contact Time

The effect of contact time on the uptake of Fe(II) and Mn(II) ions onto S-nM is shown in **Figure** ures 6. It was observed that the quantity of Fe(II) and Mn(II) removed increased with increase in contact time and was optimum at 60 min with the sorption efficiencies for Fe(II) and Mn(II) of 29.25%and 41.43%, respectively. This result may be due to the use of vacant adsorption sites on the adsorbent surface. During the initial stage of sorption, a large number of vacant surface sites were available for adsorption. After a lapse in time, the remaining vacant surface sites were occupied due to repulsive forces between the solute molecules on the adsorbent surface and the bulk phase [21].

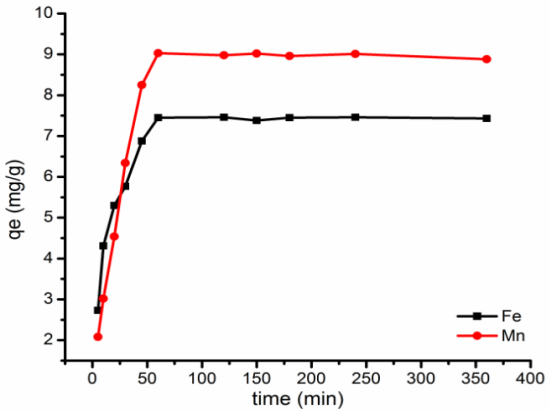

Figure . 6: Effect of contact time on the sorption capacity of Fe(II) and Mn onto S-nM (weight= 0.1g, Temp= 30±2^{0}C, pH=6)

Adsorbent Dose

Figure ures 7 shows the effect of the adsorbent dose on the sorption of Fe(II) and Mn(II) ions. The sorption efficiencies of Fe(II) and Mn(II) were found to increase exponentially with the increase in adsorbent dose up to 0.15 g. This may be due to the increase in availability of surface active sites resulting from the increased dose of adsorbent. At higher dosages, 0.15 g and 0.2 g, sorption was almost the same and at maximum as a result of complete usage of the adsorption site which reduced the tendency of the particles to adsorb anymore ions to its surface, so removal rate of heavy metal ions no longer increased [22].

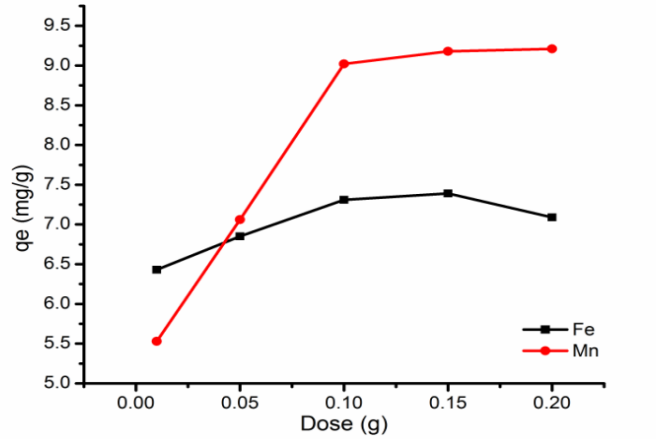

Figure . 7a: Effect of adsorbent dose on the sorption capacity of Fe(II) and Mn(II) onto S-nM (Temp= 30±2^{0}C, pH=6 for 120min)

Effect of Temperature

The effect of temperature on the adsorption process of Fe(II) and Mn(II) ions onto S-nM was studied at temperature range of 30-70 ^{o}C using 25 ml metal solutions at pH 6 and 0.1 g adsorbent dose. Increase in temperature led to increase in the removal efficiency of both Fe(II) and Mn(II) which was due to increase in number of active sites and the decrease in the thickness of the boundary layer surrounding the adsorbent [23]. Moreover, increasing temperature resulted in an increase in the rate of approach to equilibrium.

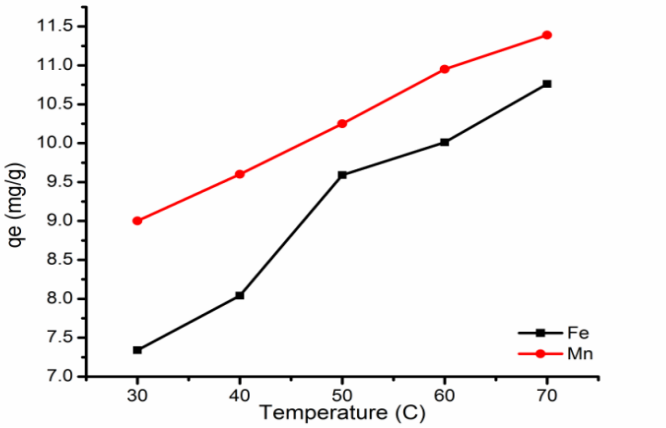

Figure . 8: Effect of temperature on the sorption capacity of Fe(II) and Mn(II) onto S-nM (dose=0.1g, pH=6 for 120min)

Adsorption Isotherm

The results are presented in **Figure** ures 19 (a – d) while the isotherm parameters are calculated and summarized in **Table** 2. The adsorption data for both Fe(II) and Mn(II) fit the isotherm models in this order: Langmuir > Freundlich > Temkin > Dubinin-Radushkevich. Adsorption data for the Fe(II) and Mn(II) onto the S-nM composite fitted more to Langmuir isotherm as shown in **Figure** . 9a with regression coefficient of 0.992 and 0.979 respectively. The good agreement of Langmuir's isotherm with the adsorption data may be due to homogenous distribution of active sites on the adsorbent since the Langmuir equation assumes that the surface is homogenous. The values of the adsorption coefficient and the monolayer capacity calculated from Langmuir equation is given in **Table** 2 and the R_L (0.053) values shows that the adsorption of Fe(II) onto S-nM composite is favorable. These facts suggest that Fe (II) and Mn(II) are adsorbed in the form of monolayer coverage on the surface of the prepared adsorbent [24]. Freundlich isotherm was able to fairly explain the adsorption process with regression coefficient of 0.895 and 0.884 for Fe(II) and Mn(II) respectively. The Freundlich constant n (2.532 for Fe(II) and 2.392 for Mn(II)) indicates that the adsorption is favorable since it lies between 1 and 10 [25]. The evaluated parameters of Temkin Isotherm model for sorption of Fe(II) onto S-nM are also presented in **Table** 2. The Temkin isotherm constant related to the heat of Sorption (b_T) was 1266.520 $Jmol^{-1}$ and the Temkin isotherm equilibrium binding constant (A_T) was 0.742 Lg^{-1} determined from the slope and intercept obtained from appropriate plot of *Qe* versus *lnCe.* The low value of the A_T also supports the physisorption process of adsorption. The adsorption data was further supported by the Dubinin-Radushkevich isotherm model with the regression value of the plot is 0.917 for Fe(II) removal and 0.649 for Mn(II) removal. Since the magnitude of E (free energy of transfer of one solute from infinity to the surface of S-nM) is less than 8 $kJmol^{-1}$, the adsorption mechanism is physisorption which further supported Freundlich and Temkin Isotherm. This finding is similar to what was obtained elsewhere in the literature [26].

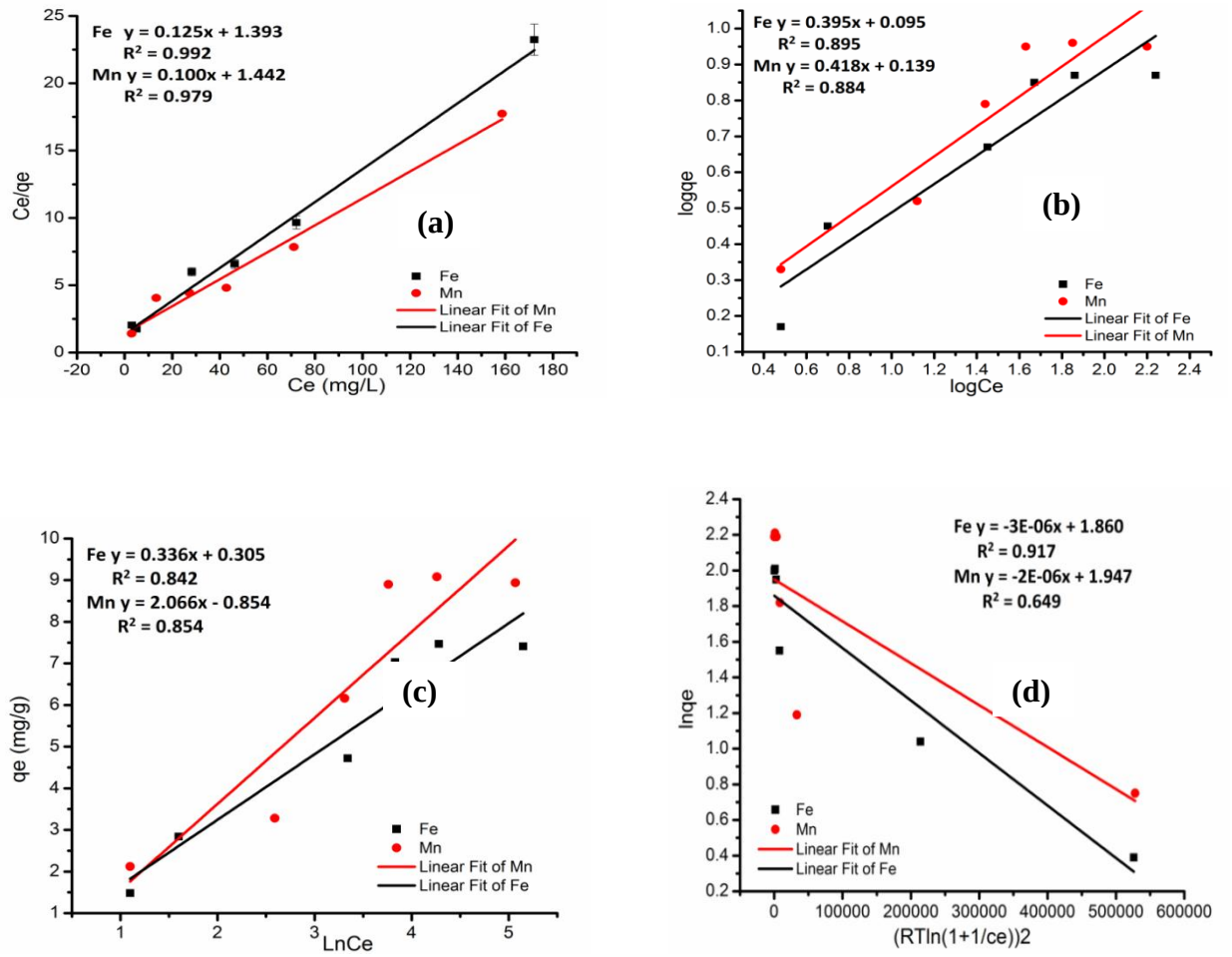

Figure 9: Langmuir (a), Freundlich (b), Temkin (c) and Dubinin Radushkevich (d) isotherm plots for the sorption of Fe(II) and Mn(II) onto S-nM

Table 2 Isotherm parameters for sorption of Fe(II) and Mn(II)

Isotherm	Parameters	Fe(II)	Mn(II)
Langmuir	Q_0(mg/g)	8.000	10.000
	K_L	0.090	0.069
	R_L	0.053	0.084
	R^2	0.992	0.979
Freundlich	K_f	1.245	1.377
	n	2.532	2.392
	R^2	0.895	0.884
Temkin	b_T	1266.520	1219.330
	A_T	0.742	0.784
	R^2	0.842	0.854
Dubinin-	B_D	$1.00x10^{-5}$	$2.00X10^{-6}$
Radushkevich	q_D	1.713	7.008
	E	223.607	500.00
	R^2	0.917	0.649

Kinetics Studies

The results of the kinetic studies of adsorption of Fe(II) and Mn(II) onto S-nM are shown in **Figure** ures 11(a-d) and the parameters are shown in **Table** 3. The adsorption data fit best Pseudo second order with a regression value of 0.999 for Fe(II) and 0.996 for Mn(II). The rate increases with increase in the concentration as result of increase in the sorption sites until a saturated point was reached. The experimental quantities of Fe(II) (7.459 mg/g) and Mn(II) (9.025 mg/g) adsorbed and the calculated quantities adsorbed (7.634 mg/g for Fe(II) and 9.434 mg/g for Mn(II)) from pseudo second-order kinetics were in close agreement. The kinetic model fit well with the adsorption process and confirm the sorption of Fe(II) and Mn(II) onto S-nM. Hence the pseudo second order kinetic reaction is the rate controlling step with some intra particle diffusion taking place. The sum of square (SSE) and the non-linear chi-square test (X^2) were used to validate the kinetic models. The lower values of SSE and X^2 is an evidence of a good and close agreement between the experimental adsorption capacity and calculated adsorption capacity. Pseudo second-order has the lowest values of SSE and X^2 for both Fe(II) and Mn(II) which suggest that the processes are well described by Pseudo second order kinetics model.

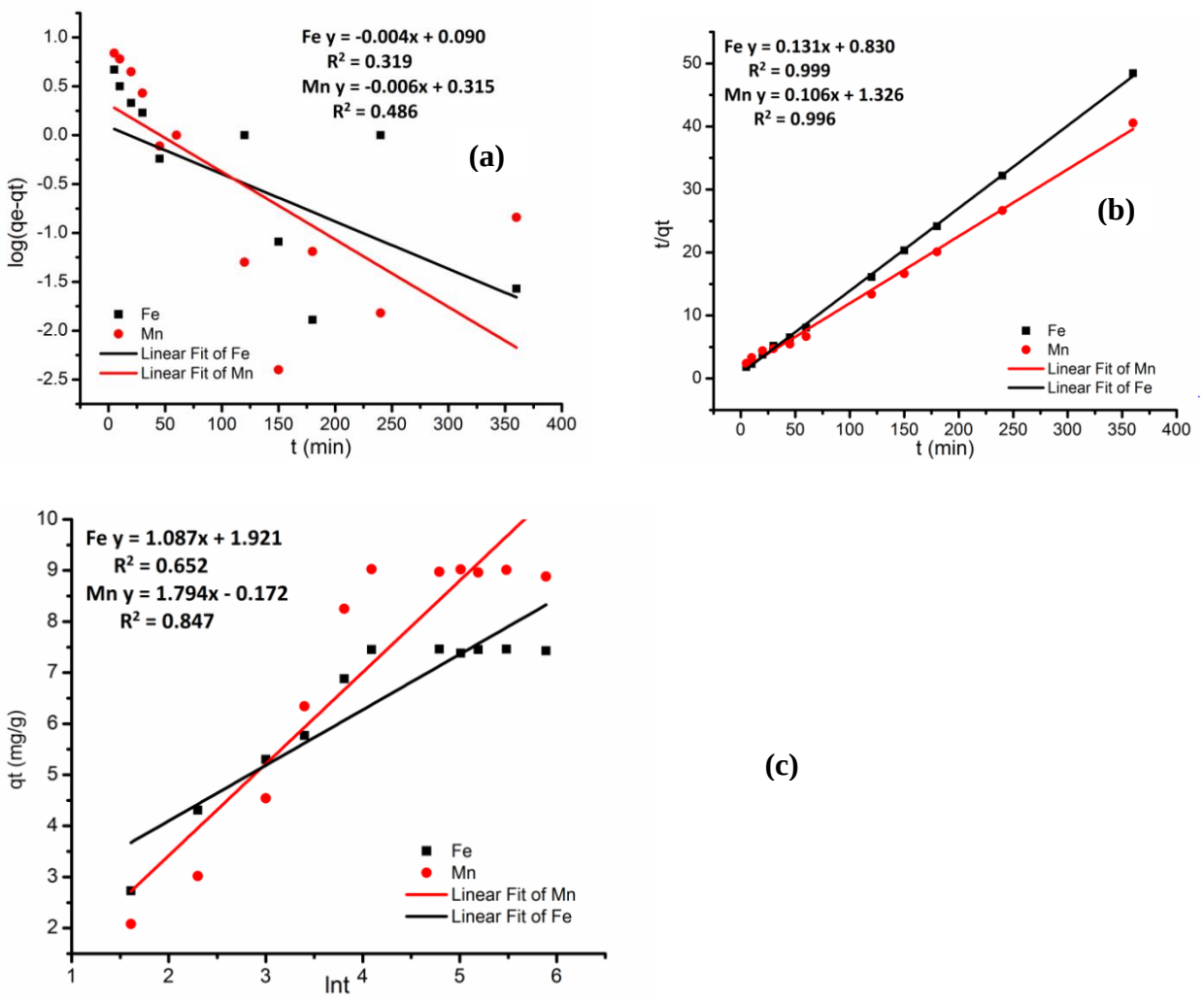

Figure . 11: Pseudo first order (a), pseudo second order (b) and Elovich (c) kinetics plots for the sorption of Fe(II) and Mn(II) onto S-nM

Table 3: Kinetics parameters for the sorption of Fe(II) and Mn(II)

Kinetics model	**Parameter**	**Fe(II)**	**Mn(II)**
Pseudo-first order	qe	1.230	2.065
	k_1	0.009	0.014
	R^2	0.319	0.486
	SSE	38.80	48.51
	X^2	31.54	23.492
Pseudo-second order	qe	7.634	9.434
	k_2	0.021	0.008
	R^2	0.999	0.996
	SSE	0.031	0.163
	X^2	0.004	0.017
Elovich	α	0.920	0.557
	β	6.364	1.631
	R^2	0.850	0.847
	SSE	0.109	0.046
	X^2	0.015	0.005

Thermodynamic studies

Temperature is another important parameter in the adsorption studies because some thermodynamic parameters such as enthalpy change (ΔH), entropy change (ΔS) and Gibbs free energy change (ΔG) could be determined. **Figure** . 13 shows the effect of temperature on the sorption of Fe(II) and Mn(II) onto S-nM. Five values of different temperature (303K, 313K, 323K, 333K and 343K) were investigated in this research. Increase in temperature led to increase in the removal efficiency of both Fe(II) and Mn(II) which was due to increase in number of active sites and the decrease in the thickness of the boundary layer surrounding the adsorbent [27]. Moreover, increasing temperature resulted in an increase in the rate of approach to equilibrium. The Van't Hoff plot of lnK versus 1/T (**Figure ure** 13) gave a straight line and the thermodynamic parameters, standard enthalpy change ΔH^o(kJ mol^{-1}) and standard entropy change ΔS(J $mol^{-1}K^{-1}$) were determined from the slope and intercept respectively. **Table** 9 shows the thermodynamic parameters of the sorption of Fe(II) and Mn(II) onto S-nM. The enthalpy change has positive values, indicating that the adsorption processes of Fe^{2+} and Mn^{2+} ions onto S-nM was endothermic with ΔH of +14349.96 $Jmol^{-1}$ for Fe(II) and +9818.83$Jmol^{-1}$ for Mn(II). The standard entropy change ΔS (46.61$Jmol^{-1}K^{-1}$ for Fe(II) and 31.24$Jmol^{-1}K^{-1}$ for Mn(II)) indicates the degree of randomness at the solid-liqiud interface during the sorption of Fe(II) and Mn(II) ions onto S-nM and the negative values of the standard Gibbs free energy ΔG indicate the feasibility and spontaneity of the adsorption process (**Table** 4). This finding agreed with the reports of other researchers [28,29].

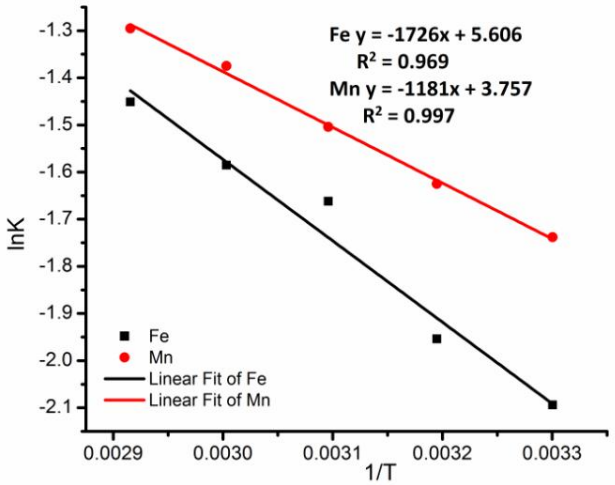

Figure . 13: A plot of lnK against 1/T for sorption of Fe(II) and Mn(II) onto S-nM

Table 4: Thermodynamic parameters for manganese (II) and iron (II)

Metals	**ΔH($Jmol^{-1}$)**	**ΔS($Jmol^{-1}$)**
Fe(II)	14349.96	46.61
Mn(II)	9818.83	31.24

Table 5: Gibb's Free Energy Values for Fe(II) and Mn(II)

Temperature(K)	**ΔG($Jmol^{-1}$) for Fe(II)**	**ΔG($Jmol^{-1}$) for Mn(II)**
303	227.65	354.42
313	-238.43	42.06
323	-704.51	-270.30
333	-1170.59	-582.65
343	-1636.38	-895.01

Removal of Fe(II) and Mn(II) from Unilorin Dam Water

The untreated Unilorin Dam Water was collected during the raining season (June) and was contacted with the prepared SiO_2-nFe_3O_4 using the optimized condition for the sorption process. From the result shown in **Figure ure** 14, the percentage removal of Fe(II) and Mn(II) were 47% and 90% respectively.

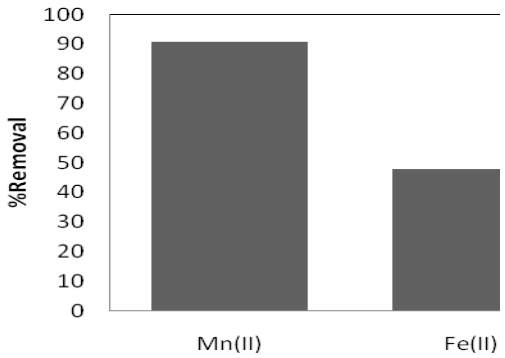

Figure 14: Removal of Fe(II) and Mn(II) from Unilorin Dam Water using SiO_2-nFe_3O_4 (Dose = 0.1g; pH = 6; time = 120min)

Conclusion

From this study, it can be concluded that the silica-nanomagnetite composite is an effective adsorbent for the removal of Fe(II) and Mn(II) ions from aqueous solutions. The quantities of Fe(II) and Mn(II) ions adsorbed were found to depend on the amount of the adsorbent, the initial concentrations of the adsorbates, the pH, contact time of adsorption and temperature. The kinetics of all the adsorption processes studied was found to be well described by Pseudo second order kinetics. From the isotherm modeling of the adsorption data, Langmuir isotherm described all the adsorption processes better than all other isotherm models that were used and the values Freundlich parameter n obtained indicated that all the adsorption processes are favourable. The values of the Gibbs free energy obtained from the thermodynamic studies further revealed that all the adsorption processes are feasible and spontaneous. Though the adsorbent effectively adsorbed all the adsorbates studied; better performance were obtained for Mn(II) than for Fe(II).

References

[1] H. Dahshan, A. M. Abd-Elall and A. M. Megahed, *J. Toxicol. Environ. Health* 76(2013), 1183−1187.

[2] Q. Tang, G. Liu, C. Zhou, H. Zhang and R. Sun, *Chemosphere* 93(2013), 2473−2479.

[3] J.A. Roth, *Biol. Res*., 39(2006), 45–57.

[4] Y. Niu, R. Qu, C. Sun, C. Wang, H. Chen, C. Ji, Y. Zhang, X. Shao and F. Bu, *J. Hazard. Mater.*, 244(2013), 276-286.

[5] R. Y. Ning, *Desalin. Water Treat.*, 12(2009), 162−168.

[6] M. Liu, Z. Tao, H. Wang, F. Zhao, Q. Sun, H. Duan, C. Luo, H. Chen, Y. Niu and H. Lee *RSC Adv.* 6(2016) 84573–84586.

[7] A. H. Nazar, Y. H. Almoeiz and A. E. Mohammed *Sci. J. of Anal. Chem.*, 1(2013), 12-20.

[8] F. A. Adekola, D. S. Hodonou and H. I. Adegoke H.I. *J. Appl. Water Sci*, 1(2014), 1-12.

[9] H. Yan, H. Li, T. Xue, K. Li, H. Yang, A. Li, S. Xiao, and R. Cheng, *ACS Appl. Mater. Interfaces*, 6(2014), 9871−9880

[10] K. Hamid, A. Abolghasem, R. Fereshteh *Int. J. Mod. Phys. Conf. Ser.*, 5(2012),160-167

[11] O.S. Ayanda, S.O. Fatoki, F. A Adekola and B. J. Ximba *J. Chem. Technol. Biot.*, 88(2013), 2201–2208.
[12] N. D. Hutson and R.T. Yang *J. Colloid Interf Sci.*,1(2000), 189.
[13] O. Hamdaoui and E. Naffrechoux *J. Hazard. Mater.*, 147(2007), 381-394.
[14] A. R. Khan, H. Tahir, F. Uddin, U. Hammed *J Appl Sci Environ Manag*, 9(2005), 29–35.
[15] A. N. Nik and M. Y. Alias, *Malaysian J. Anal. Sci.*, 11(2007), 76-83.
[16] A. Li, H. Wu, Q. Zhang, G. Zhang, C. Long, Z. Fei, F. Liu and J. Chen *Chinese J. Poly. Sci*., 22(2004), 259-267.
[17] K. A. Emmanuel and A. V. Rao, *Rasayan J. Chem.*, 1(2008), 840–852.
[18] K. A. Emmanuel and A. V. Rao *J. Chem.*, 6(2009), 693–704.
[19] J. L. Gonga, X. Y. Wanga, G. M. Zeng, L. Chen, J. H. Denga, X. R. Zhang, Q. Y. Niu *Chemical Engg J* , 185(2012) 100–107.
[20] S. R. Taffarel and J. Rubio *Minerals Engineering*, 22(2009), 336–343.
[21] J. Wongjunda and P. Saueprasearsit *Environ. Res. J.*, 4(2010), 244–250.
[22] O. Y. Onundi, A. A. Mamun, M. F. Al Khatib and Y. M. Ahmed *Int. J. Environ. Sci. Technol.*, 7(2010), 751–758.
[23] J. Hu, G. H. Chen and I. M. Lo *J. Environ. Eng*.—ASCE, 132(2006), 709–715.
[24] I. B. Singh and D. R. Singh *Indian J. Chem. Technol.* 8(2001), 487-495.
[25] K. Y. Foo and B. H. Hameed, *Chem Engg J*., 156(2010), 2–10.
[26] C. Song, S. Wu, M. Cheng, P. Tao, M. Shao and G. Gao *Sustainability*, 6(2014), 86-98.
[27] M. Doğan, A. Türkyilmaz, M. Alkan and O. Demirbaş *Desalination*, 238(2009), 257–270.
[28] Y. M. Hao, M. Chen and Z. B. Hu *J Hazard Maters*, 1849(2010), 392–399.
[29] K. P. Lisha, M. Shihabudheen and M. T. Pradeep *Chemical Engg J*, 160(2010), 432–439.